Original Article

Institution of MECHANICAL ENGINEERS
Journal of AUTOMOBILE ENGINEERING

Proc IMechE Part D:
J Automobile Engineering
2023, Vol. 237(2-3) 572–584

DOI: 10.1177/09544070221075419
journals.sagepub.com/home/pid
SAGE

Prediction of centrifugal compressor instabilities for internal combustion engines operating cycle simulation

Dmytro S Minchev[1], Oleksiy A Gogorenko[1], Roman A Varbanets[2], Yuryi L Moshentsev[1], Vaclav Píštěk[3], Pavel Kučera[3], Oleksandr M Shumylo[2] and Vladyslav I Kyrnats[2]

Abstract

Centrifugal compressors, which serve the purpose of internal combustion engines (ICE) supercharging, have a region of unstable operation. The compressor instabilities can be distinguished as rotating stall, mild, or deep surge, depending on the compression system parameters. All these types of compressor operation should be avoided for engine durability and long service life. Therefore, it is important to provide fast, stable, and correct prediction of compressor instabilities at ICE operating cycle simulation. The experimental research was conducted for an aircraft engine compressor to measure compressor performance map in the region of unstable operation, which is usually never provided by the manufacturer, and to study the compression system operation in the mild and deep surge modes. A mathematical model was developed, based on the Moore-Greitzer approach together with the modified equation of the compressor outlet pipe airflow acceleration, and integrated into the Blitz-PRO service for ICE steady and transient operation simulation. It is shown that the suggested mathematical model correlates well with the experimental data for the compressor testbench case. The application of the developed mathematical model provides fast and stable calculations and prediction of the type of compression system instability.

Keywords

Internal combustion engine simulation, centrifugal compressor surge, centrifugal compressor rotating stall, turbocharger performance maps

Date received: 8 October 2021; accepted: 4 January 2022

Introduction

Centrifugal compressors are widely used for ICE supercharging – either as a part of the turbocharger, or driven from the engine crankshaft. This type of compressor provides high efficiency combined with small size, but it also has some well-known drawbacks in terms of matching with the piston part of an engine. Firstly, centrifugal compressors need control system to achieve the desired level of supercharging pressure in the wide range of engine operation, and secondly, they have the region of unstable operation. Unstable operation modes of the centrifugal compressor are also known as compressor stall and compressor surge, affect engine efficiency and could cause damage. Compressor operation with instability should be avoided, so the prediction techniques, which could detect early stages of compressor stalling or surging, are necessary.

Simulation of the supercharged internal combustion engines (ICE) steady and transient operation is impossible without correct consideration of supercharger performance parameters.[1] In terms of ICE operating cycle synthesis, it is important to cover the whole range of possible compressor operations, including the instabilities. The last is a tough task as the rotating stall is caused by the complex of gas-dynamics reasons, which include vortex formation, while the surge or pumping depends not only on the compressor itself, but also on characteristics of the entire compression system, which include manifolds, runners, and valves.

[1]Department of Internal Combustion Engines, Plants and Technical Maintenance, National University of Shipbuilding, Mykolaiv, Ukraine
[2]Marine Engineering Department, Odessa National Maritime University, Odessa, Ukraine
[3]Institute of Automotive Engineering, Brno University of Technology, Brno, Czech Republic

Corresponding author:
Dmytro S Minchev, Department of Internal Combustion Engines, Plants and Technical Maintenance, National University of Shipbuilding, Heroiv Ukrainy Avenue, 5, Mykolaiv 54025, Ukraine.
Email: dmytro.minchev@nuos.edu.ua

This paper aims to develop the turbocharger surge prediction methods together with approaches for the correct simulation of the centrifugal compressor instabilities, based on the compressor performance maps application.

Literature review

Centrifugal compressor instabilities are usually distinguished as rotating stall and surge, which are interrelated but have different effects on the compression system. The rotating stall occurs as the airflow for the given compressor speed decreases to some level, when the small disturbance in the inlet flow causes stalling some number of compression cells, which are formed by the impeller blade. Stalling develops as the incidence angle of the inlet flow increases too much and the vortexes appear along with the compression cell. Supercharging pressure decreases gradually as well as compressor efficiency.[2] Averaged airflow remains positive during a rotating stall.

Compressor surge or pumping results in self-exiting oscillation of supercharged air pressure and air mass flow and depends on the intake receiver volume, length, and cross-area of runners (the pipe which connects the compressor and receiver and pipes, connecting the receiver and cylinders). The surge operation of the compression system could be classified as mild surge and deep surge, depending on the oscillation frequency and amplitude.

The mild surge has the oscillation frequency, close to the Helmholtz resonance frequency,[3] when the receiver is considered as the vessel with high volume, which is connected to the compressor output with the pipe. The Helmholtz frequency as the natural frequency of the oscillating system could be calculated as:

$$f_H = \frac{a_s}{2\pi}\sqrt{\frac{A_{pipe}}{V_s L_{pipe}}}, \tag{1}$$

where a_s– sonic speed at the compressor outlet temperature, A_{pipe}– the area of the pipe cross-section, L_{pipe}– the length of the pipe, V_s– receiver volume.

The deep surge in contrast to mild surge has the oscillation frequency three to five times smaller than Helmholtz frequency and is expressed as air pumping with periodic air backflow from the compressor downstream to its upstream.[4]

For centrifugal compressors the rotating stall at the inducer tips is considered as the surge predecessor, it is asymmetric due to compressor volute.[3] For the vanned diffuser compressor with a pressure increase ratio $\Pi_{cmpr} > 2$ the rotating stall could also occur in this part of the compressor[5] preceding the surge.

Papers[6,7] present a widely used approach for an axial compressor surge simulation for compressor control and unstable operation prediction issues. This method was further applied for centrifugal compressors in Fink et al.[3], Gravdahl et al.[8] One of the key elements of the method is a representation of the compressor performance characteristic consisting on three parts. The first part represents the negative slope normal compression operation curve, the second part has an S-shape and describes compressor operation in the region of unstable operation, and the third part serves to determine compressor backflow characteristic.

The non-dimensional parameter B, which describes the instability of the compression system, was also proposed by[6,7]:

$$B = \frac{1}{2}\frac{u_2}{2\pi f_H L_{pipe}}, \tag{2}$$

where u_2– circumferential impeller speed at compressor outlet.

Parameter B helps to assess the possible type of instability for given compression system: if it exceeds some critical value, the compression system will run into the surge, while beyond this critical value the rotating stall will occur.

Consideration of the compressor speed variation during surge cycle helped to match experimental results much better as it is shown in Fink et al.[3] Papers[9,10] show the gap for simulation accuracy increments applying the 1-D unsteady airflow model for the compression system flow path.

The literature review shows that some simulation approaches for a centrifugal compressor surge operation prediction were successfully developed, but it's still unclear how to adopt them for a complex ICE mathematical model. Some tough challenges should be overcome among which are stable and fast calculations together with the correct prediction of the surge operation of the compression system.

Experimental data

The set of experimental tests of centrifugal compressor behavior under different conditions was carried out on the test-bench. The test-bench can be set in three configurations, allowing examining all three types of compressor operation beyond the surge line of its performance map: "mild" surge, "deep" surge, and rotating stall.

The diagram of the testbench is given in Figure 1. The Walter M332 aircraft engine centrifugal compressor with the impeller geometry and performance data, presented in Table 1, is coupled with the electric DC motor by the planetary gear. The compressor pumps the air to the receiver through the output pipe. Two throttle plates are installed to alter the compressor airflow. The main throttle is at the exit of the receiver tank, while the auxiliary throttle is positioned close to the compressor volute outlet before the receiver tank. The auxiliary throttle serves to define the compressor

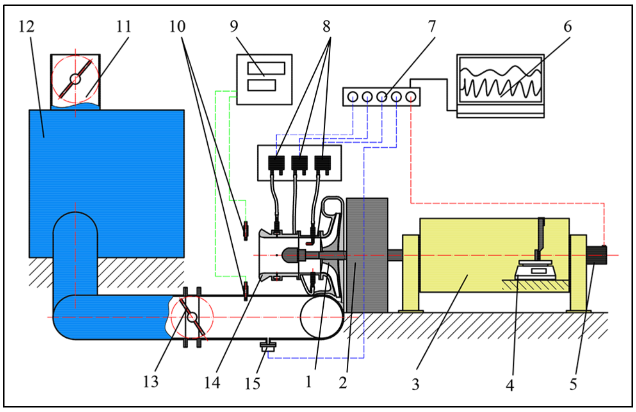

Figure 1. Centrifugal compressor testbench diagram.
1 – compressor impeller; 2 – gearbox; 3 – DC electric motor; 4 – electronic scales; 5 – tahogenerator; 6 – laptop; 7 – A/C converter; 8 – bench of Motorolla MPX5010DP pressure sensors; 9 – electronic thermometer; 10 – chromel-alumel thermocouples; 11 – main throttle; 12 – receiver tank; 13 – auxiliary throttle; 14 – airflowmeter nozzle (switchable with Siemens VDO MAF sensor); 15 – manifold air pressure sensor (Bosch 0281002401).

performance at the range of its unstable operation, and the main throttle is used to measure the standard static compressor performance map and to trigger the test-bench into the "mild" and "deep" surge mode. The "deep" surge of the compression system was possible with the short connecting pipe between the receiver and the compressor volute outlet, while the long connecting pipe was used to run the system into "mild" mode (see Figure 1).

The test-bench is equipped with necessary measuring devices. The airflow at the static operation is measured with the aid of a standard intake nozzle and optionally with the mass airflow (MAF) sensor. The Pitot tubes, one directed toward the compressor inlet and the second – to the incoming airflow, are used to detect and measure the compressor backflow under surge conditions. The detailed view of the sensors diagram is given in Figure 2. The pressure sensors of the differential type are used to measure the pressure drop levels for mentioned purposes. The compressor charging pressure is measured with the standard automotive MAP sensor, while the temperatures at the compressor inlet and outlet are measured with the chromel-alumel thermocouples and electronic thermometer. The pressure sensors signals together with the tahogenerator signal are recorded on the PC with the help of the A/D converter. Compressor speed was measured with the tahogenerator and confirmed with the acoustic spectrum analysis.[11]

Pressure sensors' accuracy was about 1% of full scale span, temperatures were measured with about 0.25°C accuracy. The accuracy of the compressor speed estimation depended rather on the speed control accuracy than on measurements errors, and could be estimated as ± 50 rpm.

The results of static measurements are presented in Figure 3. The referred impeller speed and airflow, compressor pressure increase ratio, and adiabatic efficiency are calculated as:

$$n_{cmpr.ref} = n_{cmpr}\sqrt{\frac{T_{\mathrm{int}}}{T_{ref}}},\ G_{air.ref} = G_{air}\frac{\sqrt{T_{\mathrm{int}}/T_{ref}}}{(p_0 - \Delta p_{\mathrm{int}})/p_{ref}},$$

$$\Pi_{cmpr} = \frac{p_{cmpr}}{p_0 - \Delta p_{\mathrm{int}}},\ \eta_{ad.cmpr} = \frac{T_{\mathrm{int}}\left(\Pi_{\mathrm{cmpr}}^{\frac{k-1}{k}} - 1\right)}{T_{cmpr} - T_{\mathrm{int}}}, \tag{3}$$

where p_{cmpr}, T_{cmpr}– compressor outlet pressure and temperature; p_0– barometric pressure; T_{int}– temperature at the compressor inlet; Δp_{int}– pressure drop at the compressor intake; $T_{ref} = 300\,\mathrm{K}$ and $p_{ref} = 96\,\mathrm{kPa}$ – referred temperature and pressure correspondently.

Three constant-speed curves have been measured. Each curve has two parts, considering the airflow decrement direction. The first part describes the compressor operation with the large-volume receiver tank (solid

Table 1. Compressor testbench configuration.

Parameter		Units	Large receiver	Large receiver, short pipe	Small receiver
Impeller exducer diameter	D_2	mm		150	
Impeller inducer diameter	d_1	mm		62	
Impeller hub diameter	d_{hub}	mm		27	
Number of blades	N_{blades}	–		12	
Outlet blade height	$l_{2.blade}$	mm		6	
Blade thickness	t_{blade}	mm		1.5	
Type of diffuser		–		bladeless	
Rated speed	n_{cmpr}	rpm		20,000	
Planetary gear ratio	i_{gear}	–		7.4	
Rated pressure increase ratio	Π_{cmpr}			1.25	
Receiver volume	V_s	dm^3	29	29	0.88
Compressor outlet pipe diameter	$d_{pipe.out}$	mm	68	52	52
Compressor outlet pipe length	$L_{pipe.out}$	m	1.8	0.18	0.18
Theoretical Helmholtz frequency	f_H	Hz	15.1	38.1	206.7
Theoretical B parameter	B	–	0.458	1.824	0.336

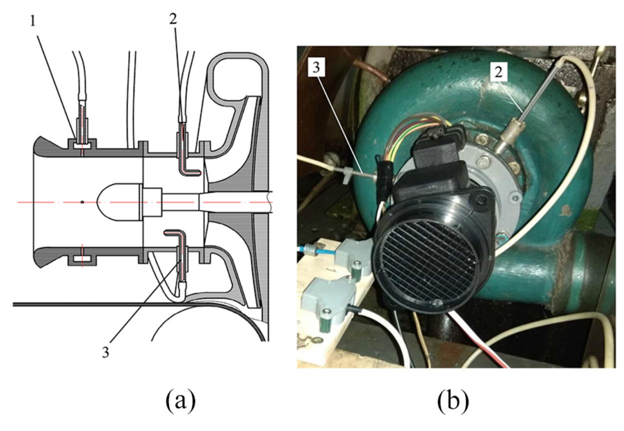

Figure 2. Compressor intake pressures measurement in detail: (a) airflowmeter nozzle configuration and (b) Siemens VDO MAF sensor configuration.

1 – ring-type 4-orifices intake static sensor; 2, 3 – Pitot-tube pressure sensors.

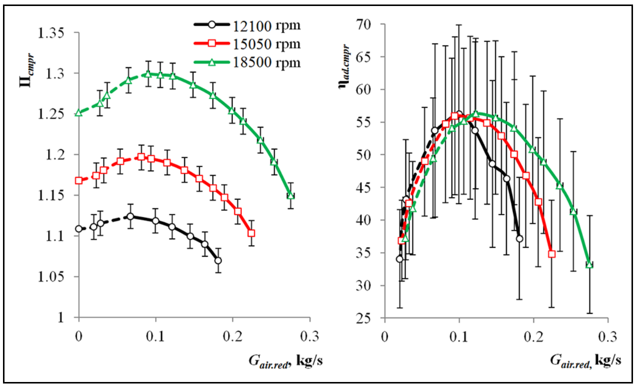

Figure 3. Measured static performance maps of the compressor with the measurements errors bars.

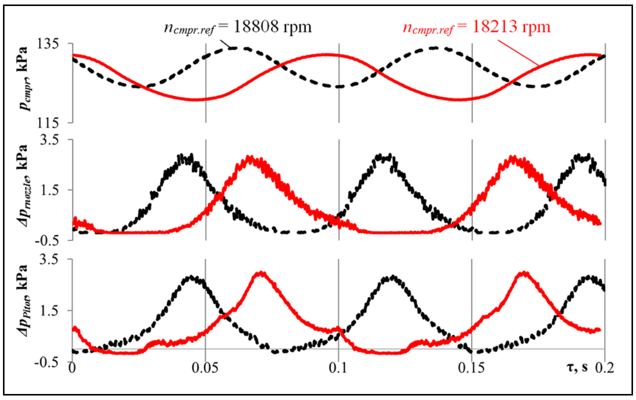

Figure 4. Averaged data for a compressor surge operation: dashed line – short pipe, "deep surge"; solid line – long pipe, "mild surge."

lines in the Figure 3) – the airflow is controlled by the main throttle plate at the receiver exit, while the auxiliary throttle at the receiver enter is opened. Further closing of the main throttle causes the surge operation of the compression system. That is why the second part of the constant-speed curve could only be measured if the compressor pumps the air into small-volume receiver. The airflow for this case is controlled by the auxiliary throttle plate at the receiver inlet and the main throttle at the receiver exit remains opened (dashed lines in Figure 3).

Error bars in the Figure 3 show the estimation of measurements accuracy. The standard approach was applied to define the errors of indirect measurements:

$$\Delta y(x_1, x_2, ..., x_n) = \sqrt{\left(\frac{\partial y}{\partial x_1}\Delta x_1\right)^2 + \left(\frac{\partial y}{\partial x_2}\Delta x_2\right)^2 + ... + \left(\frac{\partial y}{\partial x_n}\Delta x_n\right)^2},$$

where x_1, x_2, x_n – directly measured parameters, Δx_1, Δx_2, Δx_n – errors of direct measurements, Δy – absolute error of indirect measurement.

The errors of directly measured parameters are estimated basing on the sensors' accuracy and number of conducted measurements. Relatively big measurements errors for the adiabatic efficiency $\delta\eta_{ad.cmpr} = 5\%–10\%$, calculated using equation (3), are explained mainly by the accuracy of the nominator estimation at relatively small values of Π_{cmpr}.

The "mild" surge mode of the system is triggered when the auxiliary throttle is opened, while the main throttle is closed. The compressor volute outlet and the receiver tank were connected with the long pipe. The operation of the system becomes unstable with significant oscillations of airflow and pressure. A typical record lasted for about 3 s, which gives from 30 to 35 oscillations.

The "deep" surge of the compression system was measured using the short connecting pipe between the receiver tank and compressor volute outlet.

The recorded data were processed by time-averaging the signal across the oscillations:

$$Y_{av}(\tau) = \frac{1}{N_{osc}} \sum_{i=0}^{N_{osc}-1} Y_{record}\left(\frac{i}{f_{ocs}} + \tau\right), \tag{4}$$

where Y_{av}– averaged signal; Y_{record}– recorded signal; τ– the time from the oscillation start; N_{ocs}– number of recorded oscillations; f_{ocs}–oscillation frequency.

The example of experimental diagrams after data averaging could be seen in Figure 4, while Table 2 presents some parameters of the surge operation been measured. The oscillation frequency f_{ocs} slightly decreases with the compressor speed rise. The recorded "mild" surge oscillation frequency is much closer to the theoretical Helmholtz frequency, compared to the "deep" surge. The ratio between Helmholtz and actual frequencies is about 1.45 for "mild" surge and about 2.7 for the "deep" surge configuration. As the "classic" mild surge is

Table 2. Measured parameters of the compression system surge operation.

Parameter	1	2	3
		Long pipe, "mild" surge configuration	
Compressor referred speed, $n_{cmpr.ref}$, rpm	12,215	15,510	18,213
Ambient temperature, t_0, °C	16	16.2	19.1
Charge air temperature, t_{cmpr} , °C	32.2	41.1	52.5
Oscillation frequency, f_{ocs}, Hz	10.34	10.25	10.12
Actual *B* parameter	0.41	0.525	0.625
Maximum charging pressure, kPa	115.89	124.43	132.17
Minimum charging pressure, kPa	109.59	115.49	120.7
Theoretical Helmholtz frequency, f_H, Hz	14.8	14.9	15.2
Theoretical *B* parameter	0.288	0.361	0.416
		Short pipe, "deep" surge configuration	
Compressor referred speed, $n_{cmpr.ref}$, rpm	12,015	15,365	18,808
Ambient temperature, t_0, °C	15.1	15.6	15.8
Charge air temperature, t_{cmpr}, °C	31.5	42	54
Oscillation frequency, f_{ocs}, Hz	14.72	14.12	13.4
Actual *B* parameter	2.343	2.247	2.132
Maximum charging pressure, kPa	114.8	123.1	133.9
Minimum charging pressure, kPa	110.26	116.1	123.9
Theoretical Helmholtz frequency, f_H, Hz	36.12	36.76	37.45
Theoretical *B* parameter	1.178	1.479	1.769

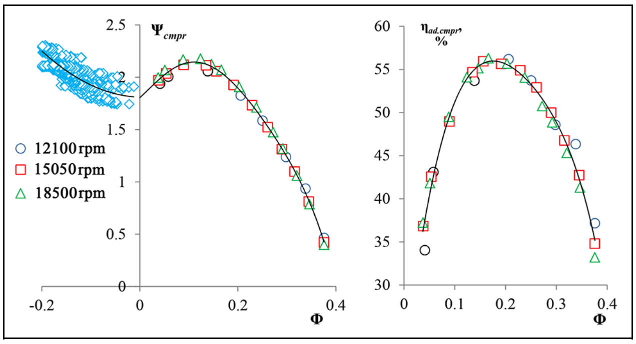

Figure 5. Dimensionless representation of compressor performance map.

supposed to have oscillations close to Helmholtz frequency, the measured "mild" surge could be classified as transitional between "classic" mild surge and "deep" surge.

To find the backflow part of the compressor characteristic the Pitot tube signal was used as it shows the air backflow explicitly. Backflow points were averaged by a polynomial equation as it could be seen in Figure 5, where experimental points are expressed in dimensionless parameters.

The dimensionless representation of the compressor flow map shows that experimental points lay on the common line as it could be seen in Figure 5. The flow coefficient Φ and the pressure rise coefficient Ψ_{cmpr} are given as:

$$\Phi = \frac{G_{air.ref}}{\rho_0 A_{pipe} u_2}; \Psi_{cmpr} = \frac{2\Delta p_{cmpr}}{\rho_0 u_2^2}, \tag{5}$$

where Δp_{cmpr} – pressures difference at the compressor outlet and inlet; ρ_0 – air density at the compressor inlet.

Thus, for the measured range of compressor speed, the compressor performance maps – both flow and efficiency – could be expressed by the single fifth order polynomial lines and the second order polynomials were applied for the backflow part of the maps.

Mathematical model development

As it was mentioned, the most effective way to consider the supercharger behavior for ICE operating cycle synthesis is to use performance maps for compressor and turbine. Blitz-PRO – non-commercial service for engineering and educational purposes with free access – applies specially prepared performance maps for compressor and turbine for this task.[12,13] The compression system unstable operation prediction is an extension of the existing routings and is also based on the supercharger performance maps.

The simulation of the ICE operating cycle has some differences in terms of supercharger instability prediction for steady and transient engine operation issues. Steady engine operation means its speed and torque (averaged by cycle) are considered constant. This type of simulations is used for engine static performance characteristics calculation, prediction of the engine heat balance, research into combustion and heat transfer processes, etc. Among these tasks, one of the important is matching the given supercharger to the engine, using its performance maps. The requirements for the compressor instability prediction could be set as following:

1. Rotating stall, "mild" and "deep" surge operation should be distinguished correctly; the amplitude

and frequency of pulsations are to be calculated with 10%–30 % accuracy.
2. Calculations should be fast and stable as the main focus is on the engine overall parameters, not on the compression system instability problem.
3. Supercharger speed variation throughout the operating cycle could be neglected.

Blitz-PRO utilizes a combination of the quasi-steady (single and two-zone) and one-dimensional unsteady approaches to describe the processes in interrelated open thermodynamic systems (OTS), which are parts of the general thermodynamic system – the engine.[14]

The equations sets include the first law of thermodynamics, mass balance, and gas state differential equations for quasi-steady OTS. The first law of thermodynamics is expressed as:

$$\left(\frac{\mathrm{d}I_{fuel}}{\mathrm{d}\varphi} + \sum_{1}^{n_1}\frac{\mathrm{d}I_j}{\mathrm{d}\varphi}\right) + \frac{\delta Q_{comb}}{\mathrm{d}\varphi} + \sum_{1}^{n_2}\frac{\delta Q_{wall.i}}{\mathrm{d}\varphi} = c_{vm}T\left(\sum_{1}^{n_1}\frac{\mathrm{d}m_j}{\mathrm{d}\varphi} + \frac{\mathrm{d}m_{fuel}}{\mathrm{d}\varphi}\right) + c_v m\frac{\mathrm{d}T}{d\varphi} + mT\frac{d(c_v)_T}{d\varphi} + p\frac{\mathrm{d}V}{\mathrm{d}\varphi}, \tag{6}$$

where $\mathrm{d}I_{fuel}/\mathrm{d}\varphi$, $\mathrm{d}I_j/\mathrm{d}\varphi$ – the rate of enthalpy change due to fuel evaporation and due to mass exchange processes, $\delta Q_{comb}/\mathrm{d}\varphi$ – heat release rate due to fuel combustion, $\delta Q_{wall.i}/\mathrm{d}\varphi$ – heat transfer rate to the walls of the system, $\mathrm{d}m_{fuel}/\mathrm{d}\varphi$, $\mathrm{d}m_j/\mathrm{d}\varphi$ – fuel mass flow and gases mass flow, n_1 – number of the interacting thermodynamic systems, involved into mass exchange process, n_2 – number of walls, involved into heat transfer process, p, T, V, m – pressure, temperature, volume, mass of the gases mixture in the OTS, c_v, c_{vm} – actual and average isochoric specific heat capacity.

The thermodynamics first law equation is completed with the mass balance equation and with the gas-state equation:

$$\mathrm{d}m = \sum_{1}^{n_1}\mathrm{d}m_j + \mathrm{d}m_{fuel}\,; pV = Z\frac{m}{\mu}RT, \tag{7}$$

where Z is compression factor, calculated by the Berthelot equation:

$$Z = 1 + \frac{9}{128}\frac{\pi}{\theta}\left(1 - \frac{6}{\theta^2}\right) \tag{8}$$

where $\pi = p/p_{crit}$, $\theta = T/T_{crit}$ relative to critical pressure and temperature.

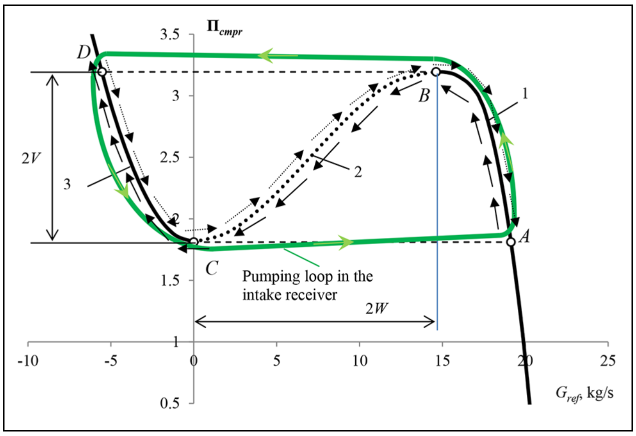

Figure 6. Compressor constant-speed line treatment for "deep" surge simulation: 1 – compressor stable operation line *AB*; 2 – compressor unstable operation region *BC*; 3 – backflow part of the constant-speed line *CD*.

The mass flow between interacting thermodynamic systems is calculated on the traditional quasi-steady nozzle approach:

$$w_{static} = \begin{cases} \sqrt{\frac{2k_1}{k_1-1}R_\mu T_1^*\left[1 - \left(\frac{p_2}{p_1^*}\right)^{\frac{k_1-1}{k_1}}\right]}, \\ \quad \text{if } \frac{p_1}{p_2} < \left(\frac{2}{k_1+1}\right)^{\left(\frac{k_1}{1-k_1}\right)}; \\ \sqrt{\frac{2k_1}{k_1+1}R_\mu T_1^*}, \text{ if } \frac{p_1}{p_2} > \left(\frac{2}{k_1+1}\right)^{\left(\frac{k_1}{1-k_1}\right)}, \end{cases} \tag{9}$$

where w_{static}– the gas flow velocity from the volume with higher pressure "1" to the volume with lower pressure "2"; k_1 is the adiabatic exponent, "*" indicates total parameters.

To consider the gas flow inertia, the pulse conservation equation applied as:

$$\frac{dw}{d\tau} = \frac{w_{static}\cdot|w_{static}| - w\cdot|w|}{2L_{dyn}}, \tag{10}$$

where L_{dyn} is the "dynamic" pipe length.

For one-dimensional OTS energy, pulse and mass conservation differential equations are applied:

$$\begin{cases} \frac{\partial\rho}{\partial\tau} + w\frac{\partial\rho}{\partial x} + \rho\frac{\partial w}{\partial x} = -\lambda_{fr}\frac{w|w|}{2d}; \\ \frac{\partial w}{\partial\tau} + w\frac{\partial w}{\partial x} + \frac{1}{\rho}\frac{\partial p}{\partial x} = -w\rho\frac{\mathrm{d}\ln f}{\mathrm{d}x}; \\ \frac{\partial S}{\partial\tau} + w\frac{\partial S}{\partial x} = \frac{1}{T}\left(\lambda_{fr}\frac{|w^3|}{2d} - \frac{4\alpha}{\rho d}(T_{wall} - T)\right); \\ S - S_{no} = \frac{R_\mu}{k-1}\ln\frac{p/p_{no}}{\left(\rho/\rho_{no}\right)^k}, \end{cases} \tag{11}$$

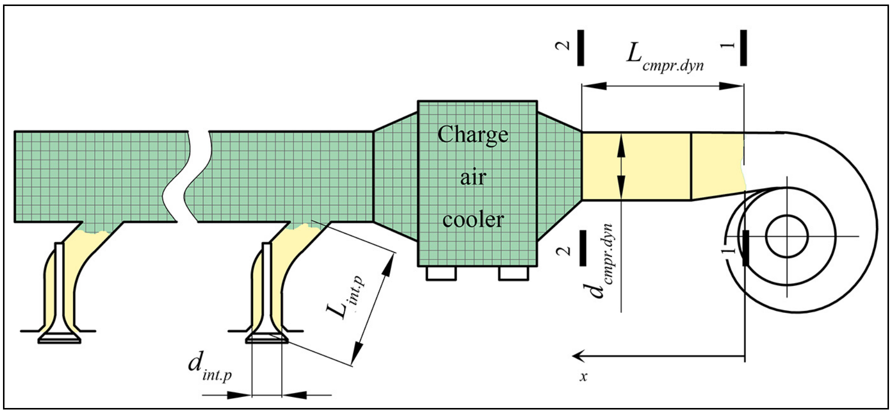

Figure 7. Intake receiver diagram, the checkered region relates to the "steady" part of the manifold, while the other filled regions relate to the receiver parts, where gas dynamics effects are significant.

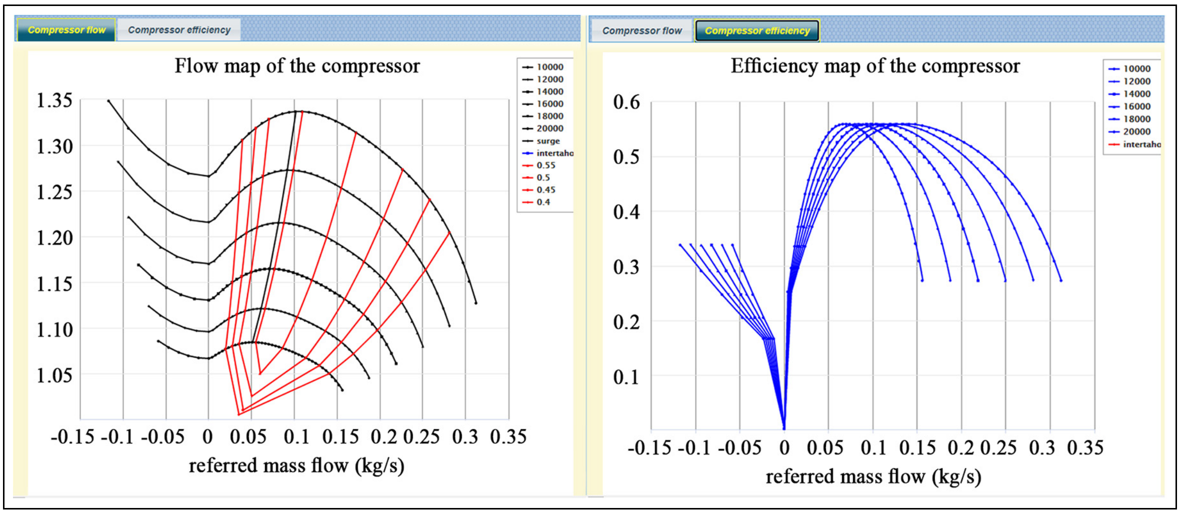

Figure 8. The Walter 332 aircraft engine centrifugal compressor performance maps as used in Blitz-PRO environment (axis labels are enlarged for visibility).

where λ_{fr}– coefficient of friction; α– heat transfer coefficient from gas to the pipe wall; T_{wall}– pipe wall temperature; T– gas temperature; S– entropy; "$_{no}$"– referred to normal conditions; d– pipe diameter; k– adiabatic exponent.

The solution for the combination of equations sets for all interrelated OTS is numerical: the user can choose between the simple Euler and second order implicit Runge-Kutta method.[15] A numerical solution, obviously, requires the set of initial conditions and then the iterative calculations to obey the target level of calculations accuracy. The typical number of such iterative approaches generally is between 20 and 300 iterations.

The supercharger instant parameters should be determined for each computational step, among them are: the compressor pressure increase ratio Π_{cmpr}, the airflow G_{air}, and the adiabatic efficiency $\eta_{cmpr.ad}$. All these parameters are calculated from the supercharger performance maps (see Figure 8 for the example).

The compressor constant-speed line treatment is presented in Figure 6. Constant speed line consists of three parts: stable part AB, unstable part BC, and backflow part CD. The stable part AB is generally available from the manufacturer's documentation and should be extrapolated up to the chocking limit, while the unstable and backflow parts are absent and could could be obtained either from special experiments or using approximate equations. The unstable part BC in case of experimental data absence could be assumed with the equations[8,16]:

$$\prod^{BD}_{cmpr} = \prod^{D}_{cmpr} + \frac{3V}{2W^2}G^2_{ref} - \frac{V}{2W^3}G^3_{ref} \tag{12}$$

$$\prod^{C}_{cmpr} = \left(1 + \frac{(\omega_{TC}/2)^2}{2c_pT_0}\left(D_2^2 - d^2_{1.av}\right)\right)^{\frac{k}{k-1}}, G^C_{ref} = 0, \tag{13}$$

where ω_{TC}– compressor speed; T_0– air temperature at the compressor inlet; D_2, $d_{1.av}$– compressor impeller exducer and average inducer diameters; parameters V and W, also presented in Figure 6, are calculated from the measured Π_{cmpr}, $G_{air.ref}$ of point B and estimated value of Π_{cmpr} for point C.

While the compressor operates in stable mode, its parameters are taken from the line AB, following the variation of intake receiver pressure and airflow. The loop in Figure 6 shows the intake receiver transient pressure change under deep-surge conditions when the throttle is closed to such degree, that the extremum point B is reached, so the compressor switches to its positive slope part of the constant-speed line (BC) and then transits to the backflow part CD. Compressor airflow reverse causes a fast drop of the receiver pressure and the compressor returns to its negative slope part AB of the characteristic, passing through the part AB. But, as the pressure in the receiver exceeds the value for point B, the next loop starts.

The key question for the deep and mild surge operation simulation is to define correctly the instantaneous airflow of the compressor. The typical ICE charging system diagram, presented in Figure 7, consists of the receiver plenum, intake pipes or runners, charge air cooler, and compressor. In the “steady” part of the manifold the gas-dynamics effects could be neglected and the parameters are calculated using standard 0D equations set. For the intake runners and the compressor outlet pipe the gas-dynamic effects should be considered.

A simplified approach could be developed using the pulse conservation equation for 1D unsteady ideal gas flow:

$$\int_{w_1}^{w_2} w\mathrm{d}w + \int_{x_1}^{x_2} \frac{\partial w}{\partial \tau}\mathrm{d}x = -\int_{p_1}^{p_2} \frac{1}{\rho}\mathrm{d}p, \tag{14}$$

assuming $\rho = \text{const}$ and $\mathrm{d}w/\mathrm{d}\tau$ the same across the pipeline

$$\frac{w_2^2 - w_1^2}{2} + \frac{\mathrm{d}w}{\mathrm{d}\tau} L_{cmpr.dyn} = -\frac{p_2 - p_1}{\rho};$$

$$\frac{\mathrm{d}w}{\mathrm{d}\tau} = -\frac{\frac{p_2 - p_1}{\rho} + \frac{w_2^2 - w_1^2}{2}}{L_{cmpr.dyn}}. \tag{15}$$

Assuming $w_2 = w_1$ we get the equation of incompressible flow: so the term $1/2(w_2 - w_1)$ contains the unsteady effects of gas flow. As it could be seen further, the consideration of unsteady effects is vital for a rotating stall mode simulation. To consider these effects under the simplified model frame, the function $f_{unst} = f(\tau)$ was suggested:

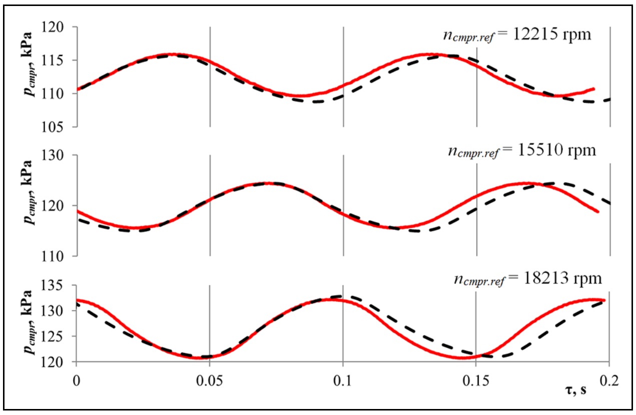

Figure 9. Simulated (dashed lines) and experimental (solid lines) diagrams of the compression system under “mild” surge conditions.

$$f_{unst}(\tau) = -b_{adj}\frac{\mathrm{d}(\Delta p)}{\mathrm{d}\tau}; \frac{\mathrm{d}w}{\mathrm{d}\tau} = -\frac{\frac{p_2 - p_1}{\rho} + f_{unst}(\tau)}{L_{cmpr.dyn}} \tag{16}$$

where $\Delta p = p_2 - p_1$; b_{adj} is the adjustment factor, which is proposed as:

$$b_{adj} = 0.01\frac{2\pi f_H}{B} \tag{17}$$

Analysis of b_{adj} equation shows that the greatest contribution of $f_{unst}(\tau)$ should be expected for the compression system with high f_H and small B– which is common to the rotating stall operation mode.

Mathematical model verification

To verify the developed mathematical model the comparison between experimental and simulated results was made. The compressor test-bench simulation mode was added in Blitz-PRO. Figure 8 shows the extrapolated and interpolated experimental Walter 332 compressor performance maps, generated using experimental data, presented in Figures 3 and 5.

The physical meaning of the compressor adiabatic efficiency in the negative flow range is considering it as running in the “turbine” mode, producing positive power. These maps were used for simulations.

The “mild” surge simulations and experimental results comparison could be seen in Figures 9 and 11a. From Table 3 it could be noticed that the error of predicted oscillation frequency is below 10% and for the maximum and minimum pressure levels – less than 1%. It is important, that simulations predicted correctly step decrement of f_{osc} as the compressor speed rises.

As for the “deep” surge – the same information is presented in Figures 10 and 11(b). Simulations accuracy is worse, comparing to the “mild” surge conditions: the

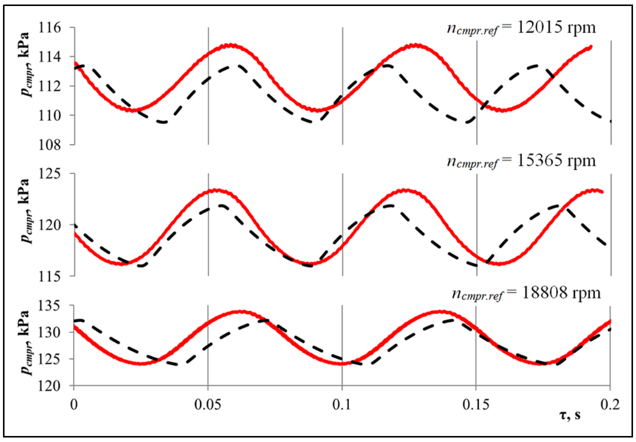

Figure 10. Simulated (dashed lines) and experimental (solid lines) diagrams of the compression system under "deep" surge conditions.

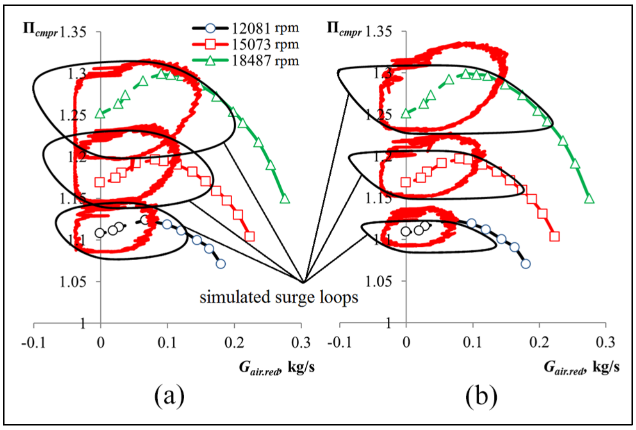

Figure 11. Simulated and experimental surge loops: (a) "mild" surge and (b) "deep" surge.

error for oscillation frequency is about 7%–20% and the pressures level prediction error is less than 1.5%. At the same time the much stepper decrement of the f_{ocs} with the compressor speed rise (compared to the "mild" surge case) is obtained in simulations, which correlates well with the experimental results.

As for the rotating stall mode of compressor operation, the importance of the function $f_{unst} = f(\tau)$, calculated in accordance with equation (16), considering unsteady effects if illustrated in Figure 12. Application of $f_{unst}(\tau)$ helps to obtain stable operation of the compression system under rotating stall conditions, which is additionally illustrated for the Cummins ST50 turbocharger testbench simulation according to Fink et al.[3]

It is necessary to underline, that all simulation results for the "mild" and "deep" surge operation mode as well as for the rotating stall mode are made with the same model setup – there is no need to tune $f_{unst}(\tau)$ for different modes of system operation.

Simulation of ICE supercharging system unstable operation

As a result of the experimental and theoretical research, the developed method of centrifugal compressor unstable operation prediction was applied to the Blitz-PRO service. The ICE operating cycle synthesis in terms of supercharging system matching generally passes three steps:

1. Estimation of the compressor G_{air} and Π_{cmpr} for a number of engine operating points using the approximate values of the compressor and turbine efficiencies (considered constant throughout the operating cycle), describing compressor as equivalent diffuser and turbine as equivalent nozzle. At this step, the supercharger performance maps are switched off.
2. Matching the supercharger performance maps using the parameters, calculated in the previous step. At this step, the rough estimation of compressor and turbine maps matching is to be made, so it's very important to conduct fast and stable calculations of the engine operating cycle even if the compressor operating point appears in the region of unstable operation.
3. Accurate matching of the supercharger performance maps, including estimation of possible compression system unstable operation. At this stage, the type and general parameters of the possible compressor rotating stall, "mild" or "deep" surge operation should be determined.

Table 3. Simulation and experimental results comparison.

Parameter	Experiment	Simulation	Experiment	Simulation	Experiment	Simulation
Long pipe, "mild" surge configuration						
Compressor speed, $n_{cmpr.ref}$, rpm	12,215		15,510		18,213	
Oscillation frequency, f_{ocs}, Hz	10.34	9.609	10.25	9.346	10.12	9.124
Maximum charging pressure, kPa	115.89	115.63	124.43	124.37	132.17	132.78
Minimum charging pressure, kPa	109.59	108.76	115.49	114.96	120.7	121.01
Short pipe, "deep" surge configuration						
Compressor speed, $n_{cmpr.ref}$, rpm	12,015		15,365		18,808	
Oscillation frequency, f_{ocs}, Hz	14.72	17.885	14.12	15.802	13.4	14.371
Maximum charging pressure, kPa	114.8	113.4	123.1	121.85	133.9	132.2
Minimum charging pressure, kPa	110.26	109.5	116.1	116.0	124.0	123.9

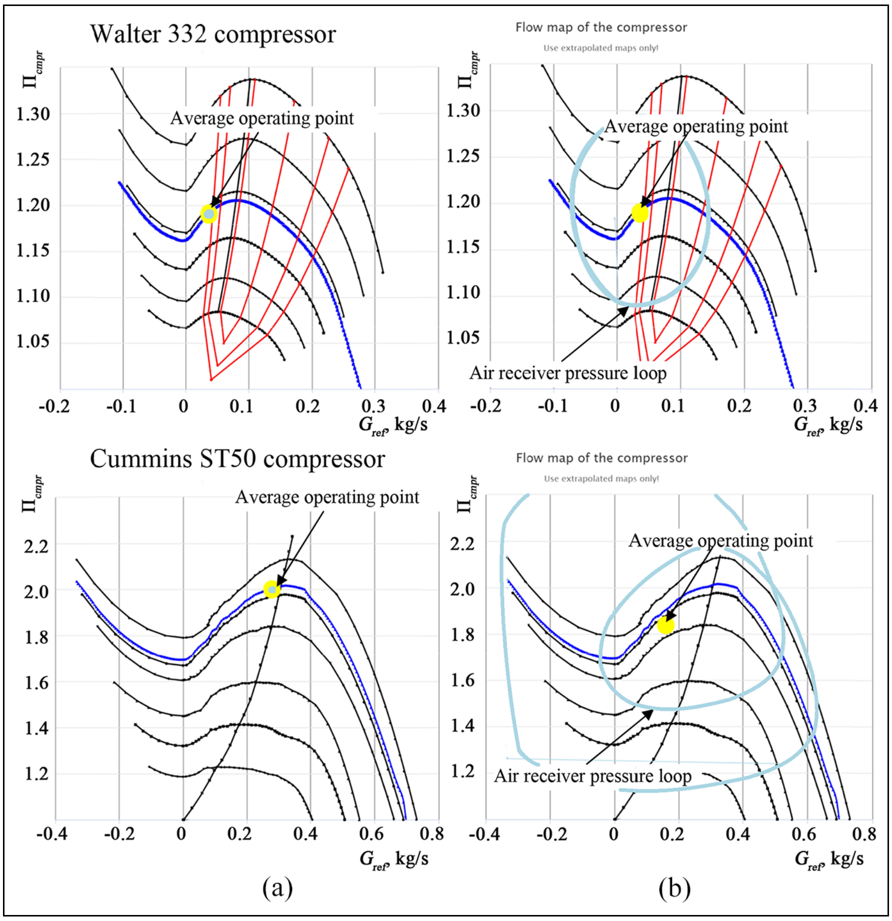

Figure 12. Small-volume configuration of the charge system (rotating stall mode, auxiliary throttle closed): with (a) and without $f_{unst} = f(\tau)$ (b) in equation (16).

To provide the ability to alter the speed and computational stability of calculations, the multiplier μG_{surge} is proposed for the compressor map treatment setup. It could be set in two ways: (1) $0 < \mu G_{surge} < 1$ to scale the unstable branch of the compressor characteristic; (2) $\mu G_{surge} = 0$ to turn calculations into "stable" mode. The following equation is used for scaling the unstable branch of the constant-speed line as it is shown in Figure 13, line 2:

$$\prod_{cmpr}' = \prod_{cmpr}^{B} - \mu G_{surge}\left(\prod_{cmpr}^{B} - \prod_{cmpr}\right) \qquad (18)$$

where Π_{cmpr}^{B}– the pressure increase ratio at the surge limit (point B).

Obviously, with the help of μG_{surge} it is possible to change the surge loops and to set up compressor performance maps closer to experimental data.

For fast and stable calculations the user can also choose $\mu G_{surge} = 0$, which switches the unstable part of the compressor performance map to the hyperbolic curve as it is shown in Figure 13, line 3, according to the equation:

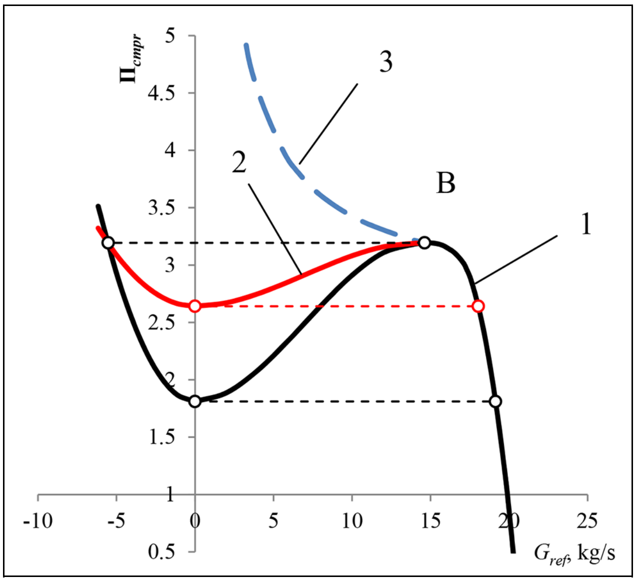

Figure 13. Constant-speed line of the compressor for different values of μG_{surge}: (1) $\mu G_{surge} = 1$, (2) $\mu G_{surge} = 0.4$, and (3) $\mu G_{surge} = 0$.

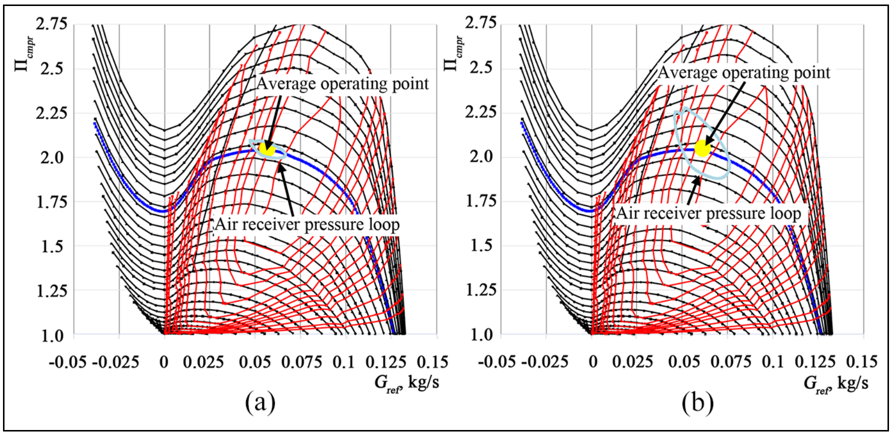

Figure 14. Simulated instantaneous compressor operating loop and averaged operating point with multiplier $\mu G_{surge} = 0$ applied (instability switched-off): (a) large receiver, $B = 1.14$ and (b) small receiver, $B = 0.293$.

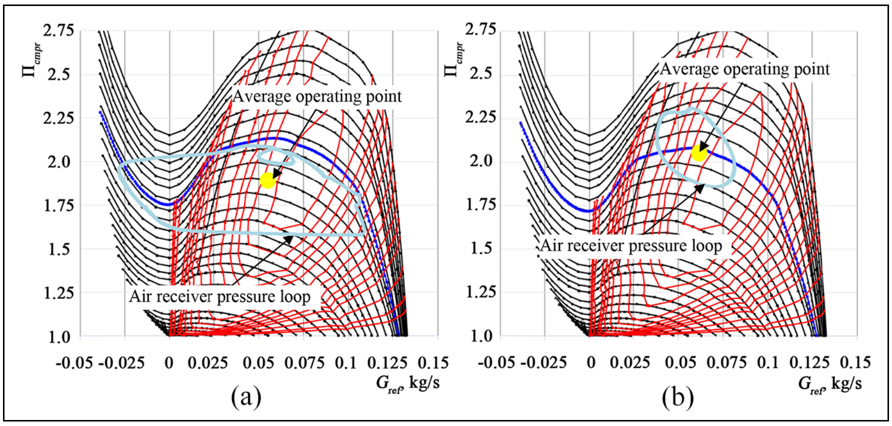

Figure 15. Simulated compressor operation with the instability consideration switched-on (multiplier $\mu G_{surge} = 1$ applied). The engine speed and load are similar to Figure 14: (a) large receiver, $B = 1.14$ and (b) small receiver, $B = 0.293$.

$$G_{ref} = \frac{G_{ref}^{B}}{2\left|\left(\prod_{cmpr} - \prod_{cmpr}^{B}\right) + 1\right|} \tag{19}$$

As an example, the simulations of the four cylinder automotive 1.9 l displacement volume diesel engine with the bore/ stroke equal to 7.95/9.55 cm are presented. The operating point of the maximum torque (57 kW at 1900 rpm) was examined. Turbocharger performance maps, used for the calculations, are based on the Garrett 1749 V turbocharger manufacturer's data. Two different air receivers were tested: large receiver with volume $V_s = 3.45$ l and the small one with $V_s = 0.7$ l. The compression system instability factor, calculated with the equation (2), for the large and small receiver is $B = 1.14$ and $B = 0.293$ respectively.

The calculations results with the compressor instability range switched-off (by applying $\mu G_{surge} = 0$) are shown in Figure 14. The averaged operating points for both small and large air receivers are very similar, while the receiver instantaneous pressure and mass flow variations are, naturally, much greater for the small volume receiver. It is important to notice, that averaged operation point lies very close to the compressor constant-speed line peak, which may cause some sort of compressor unstable operation.

To check this possibility the compressor unstable operating range was switched-on by application $\mu G_{surge} = 1$. As it could be seen from Figure 15, the large volume compression system runs into the surge mode, while the small volume system remains stable. Detailed comparison of the processes in the compression system is given in Figure 16: the large volume receiver suffers a typical deep surge at the oscillation frequency $f_{osc} \approx 15.8$ Hz.

Operating point 57 kW at 1900 rpm of 1.9 l automotive diesel engine on the centrifugal compressor performance map with $\mu G_{surge} = 1$ (instability switched-on): (a) large receiver, $B = 1.14$ and (b) small receiver, $B = 0.293$.

Conclusions

Supercharging device operation with compressor instability is highly undesirable and should be avoided at any cost in the whole range of internal combustion

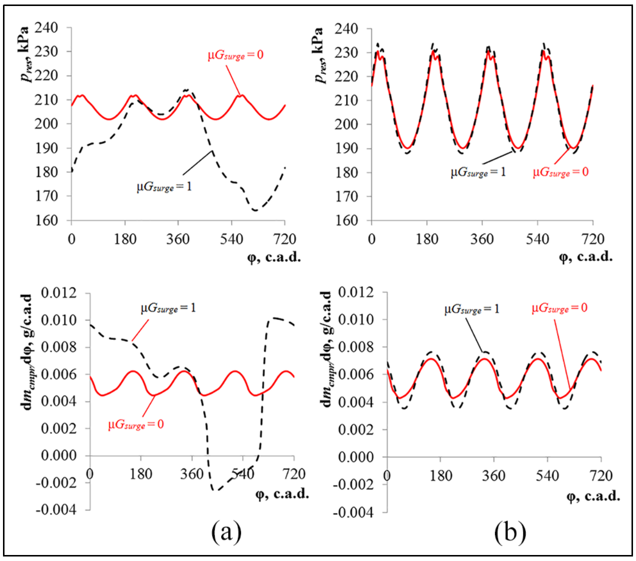

Figure 16. Intake receiver pressure and turbocharger air mass flow diagrams: (a) large receiver, $B = 1.14$ and (b) small receiver, $B = 0.293$.

engine speed and load. At the same time, significant difference between types of centrifugal compressor instabilities should be mentioned. Under the rotating stall conditions, the noticeable oscillation of intake receiver pressure and compressor mass flow are rather absent. The mild surge operation of the compression system could be characterized by compressor outlet pressure pulsations without airflow reversing and with oscillation frequency close to Helmholtz resonance. The deep surge operation is followed by airflow reversing together with loud pumping at the frequency two to three times smaller than the Helmholtz resonance. In terms of compressor and engine damage the most dangerous is deep surge mode, while the less detrimental is the rotating stall mode, which is still undesirable due to compressor overheating and blades overloading.

The experimental study on the Walter 332 engine mechanical centrifugal compressor test-bench confirmed that the mode of compressor instability is determined both by the characteristic of the compressor and by parameters of the air receiver and connecting pipes. All three modes of compressor unstable operation were measured and recorded, providing important data for mathematical model development and calibration.

In terms of ICE operating cycle simulation, it is highly important to be able to predict the compressor instability for the given stable or transient mode of engine operation and given configuration of air receiver. It is also necessary to see distinctions between the impacts of different modes of compressor unstable operation on the engine parameters.

The extrapolated performance maps of centrifugal compressor extended to the regions of compressor rotating stall and backflow operation according to Moore-Greitzer method were adopted to solve the problem of the compressor instability prediction. The pulse conservation equation for the airflow in the compressor outlet pipe was modified to consider the gas compressibility effects by adopting the special stabilizing function. This function has a negligible effect on calculations when the system operates under mild or deep surge conditions and helps to get a proper compressor operation under the rotating stall mode.

The mathematical model for centrifugal compressor unstable operation was integrated into the Blitz-PRO on-line ICE operating cycle computation service and was verified by comparison of calculation results with the experimental data for both Walter 332 engine compressor and Cummins ST50 turbocharger.[3] For the mild surge, the accuracy of calculations is about 1% in terms of charge pressure level pulsations prediction and about 10% in terms of oscillation frequency, while for the deep surge corresponding values are about 1.5% and 7%–20%. It is important that the model is also able to predict correct compressor behavior under rotating stall conditions.

Application of this model for ICE steady operation simulation proves the ability of compressor instability calculation for different types of compression system configuration. To provide the ability of model adjustments the tuning multipliers were also provided for the user, which help to turn the model into the stable mode or adjust the level of compressor instability.

Declaration of conflicting interests

The author(s) declared no potential conflicts of interest with respect to the research, authorship, and/or publication of this article.

Funding

The author(s) disclosed receipt of the following financial support for the research, authorship, and/or publication of this article: The authors gratefully acknowledge funding from the Specific research on BUT FSI-S-20-6267, National University of Shipbuilding, and Odessa National Maritime University for the support.

ORCID iDs

Dmytro S Minchev, https://orcid.org/0000-0002-5960-3063
Oleksiy Gogorenko, https://orcid.org/0000-0002-9157-6659
Vaclav Píštěk, https://orcid.org/0000-0003-2863-0226
Pavel Kučera, https://orcid.org/0000-0001-9652-9897

References

1. Minchev DS, Varbanets RA, Alexandrovskaya NI, et al. Marine diesel engines operating cycle simulation for diagnostics issues. *Acta Polytechnica* 2021; 61(3): 435–447.
2. Day IJ. Stall inception in axial flow compressors. *J Turbomach* 1993; 115(1): 1–9.

3. Fink DA, Cumpsty NA and Greitzer EM. Surge dynamics in a free-spool centrifugal compressor system. *J Turbomach* 1992; 114(2): 321–332.
4. Day IJ. Axial compressor performance during surge. *J Propulsion Power* 1994; 10: 329–336.
5. Zhao Y, Xi G, Zou H, et al. Experimental investigation of transient characteristics of mild surge and diffuser rotating stall in a centrifugal compressor with vaned diffuser. *Sci China Technol Sci* 2020; 63: 1212–1223.
6. Greitzer EM and Moore FK. A theory of post-stall transients in axial compression systems. Part I: Development of equations. *J Eng Gas Turbine Power* 1986; 108(1): 68–76.
7. Greitzer EM and Moore FK. A theory of post-stall transients in axial compression systems. Part II: Application. *J Eng Gas Turbine Power* 1986; 108(2): 231–239.
8. Gravdahl J, Willems F and Egeland O. Modeling for surge control of centrifugal compressors: comparison with experiment. In: *Proceedings of the 39th IEEE conference on decision and control*, Sydney, NSW, Australia, 12–15 December 2000, paper no. 00CH37187, pp.1341–1346.
9. Dehner R, Selamet A, Keller P, et al. Simulation of deep surge in a turbocharger compression system. In: *ASME turbo expo 2012: turbine technical conference and exposition*, Copenhagen. Denmark, paper no. GT2012-69124, pp.767–780.
10. Dehner R, Selamet A, Keller P, et al. Simulation of mild surge in a turbocharger compression system. *SAE Int J Engines* 2010; 3(2): 197–212.
11. Varbanets R, Fomin O, Píštěk V, et al. Acoustic method for estimation of marine low-speed engine turbocharger parameters. *J Mar Sci Eng* 2021; 9(3): 321.
12. Píštěk V, Kučera P, Fomin O, et al. Effective mistuning identification method of integrated bladed discs of marine engine turbochargers. *J Mar Sci Eng* 2020; 8(5): 379.
13. Minchev DS, Moshentsev YL and Nagirnyi AV. Extrapolation of turbocharger radial turbine characteristics. *Aerosp Eng Technol* 2011; 10(87): 173–133.
14. Minchev DS. User's manual. Blitz-PRO by D. S. Minchev, http://blitzpro.zeddmalam.com/extra/Tutorial/Help.pdf (accessed 21 September 2021).
15. Minchev DS and Nagirnyi AV. Application of the computational mesh with variable time step for ICE operating cycle synthesis. *Herald Aeroenginebuild* 2017; 1: 32–38.
16. Meuleman CHJ. *Measurement and unsteady flow modelling of centrifugal compressor surge*. Eindhoven: Technische Universiteit Eindhoven, 2002.

Appendix

Notations

f_{ocs}	oscillation frequency
f_H	Helmholtz resonator frequency
G_{air}	compressor airflow
ICE	internal combustion engine
n_{cmpr}	compressor speed
OTS	open thermodynamic system
$\eta_{cmpr.ad}$	compressor adiabatic efficiency
Φ	compressor flow coefficient
τ	time
Π_{cmpr}	compressor pressure increase ratio
Ψ_{cmpr}	compressor pressure rise coefficient